ISSN 2472-1972

Effects of an ActRIIB.Fc Ligand Trap on Cardiac Function in Simian Immunodeficiency Virus-Infected Male Rhesus Macaques

Wen Guo,[1] Karol M. Pencina,[1]* Thiago Gagliano-Jucá,[1]* Ravi Jasuja,[1] Nancy Morris,[2] Karyn E. O'Connell,[2] Susan Westmoreland,[2] and Shalender Bhasin[1]

[1]Research Program in Men's Health: Aging and Metabolism, Boston Claude D. Pepper Older Americans Independence Center, Brigham and Women's Hospital, Harvard Medical School, Boston, Massachusetts 02115; and [2]Division of Comparative Pathology, New England Primate Research Center, Southborough, Massachusetts 01772

*These authors contributed equally to this study.

An important safety consideration in the use of antagonists of myostatin and activins is whether these drugs induce myocardial hypertrophy and impair cardiac function. The current study evaluated the effects of a soluble ActRIIB receptor Fc fusion protein (ActRIIB.Fc), a ligand trap for TGF-β/activin family members including myostatin, on myocardial mass and function in simian immunodeficiency virus (SIV)-infected juvenile rhesus macaques (*Macaca mulatta*). Fourteen pair-housed, juvenile male rhesus macaques were inoculated with SIVmac239; 4 weeks postinoculation, they were treated with weekly injections of 10 mg/kg ActRIIB.Fc or saline for 12 weeks. Myocardial mass and function were evaluated using two-dimensional echocardiography at baseline and after 12 weeks. The administration of ActRIIB.Fc was associated with a significantly greater increase in thickness of left ventricular posterior wall and interventricular septum both in diastole and systole. Cardiac output and cardiac index increased with time, more in animals treated with ActRIIB.Fc than in those treated with saline, but the difference was not statistically significant. The changes in ejection fraction, fractional shortening, and stroke volume did not differ significantly between groups. The changes in end-diastolic and end-systolic volumes did not differ between groups. In addition to a large reduction in IGF1 mRNA expression in the ActRIIB.Fc-treated animals, complex changes were detected in the myocardial expression of proteins related to calcium transport and storage. In conclusion, ActRIIB.Fc administration for 12 weeks was associated with increased myocardial mass but did not adversely affect myocardial function in juvenile SIV-infected rhesus macaques. Further studies are necessary to establish long-term cardiac safety.

Freeform/Key Words: AIDS, HIV, echocardiography, myocardial hypertrophy, myostatin antagonist, nonhuman primate

Observations that naturally occurring inactivating mutations of the myostatin gene are associated with increased muscle mass [1–3] have stimulated substantial pharmaceutical efforts to develop drugs that inhibit myostatin action or signaling through the ActRIIB receptor to treat and prevent the loss of muscle mass and function during aging and chronic

Abbreviations: ActRIIB.Fc, ActRIIB receptor Fc fusion protein; EF, ejection fraction; FS, fractional shortening; LV, left ventricular; PhLB, phospholamban; PKA, protein kinase A; SERCA, sarcoplasmic calcium ATPase.

Received 10 April 2018
Accepted 22 May 2018
First Published Online 25 May 2018

August 2018 | Vol. 2, Iss. 8
doi: 10.1210/js.2018-00099 | Journal of the Endocrine Society | 817–831

illness, such as that associated with HIV infection, chronic obstructive lung disease, injury, or end-stage renal disease [4–6]. A number of inhibitors of myostatin and activins that block signaling through the ActRIIB receptor are undergoing efficacy trials in humans for these and other indications [7–9]. An important safety issue with respect to the long-term therapeutic applications of these drugs is whether these compounds induce myocardial hypertrophy and impair cardiac function [10]. The aim of this investigation was to determine the effects of an ActRIIB ligand trap, an inhibitor of myostatin, activins, and some other members of the TGF-β superfamily, on measures of myocardial mass and function using a primate model of simian immunodeficiency virus (SIV)-induced weight loss and muscle wasting [11].

Myostatin is expressed in the myocardium [12], and its myocardial expression is upregulated in cardiac ischemia and heart failure [12, 13]. Furthermore, myostatin has been reported to inhibit IGF-1–stimulated proliferation and hypertrophy of cardiomyocytes [14–17]. Therefore, inactivation of myostatin would be expected to increase myocardial mass. However, previous studies of the effects of genetic disruption of myostatin on the heart in rodents have yielded conflicting results [16–22]. Some studies have reported myocardial hypertrophy in myostatin-null mice [17–19], but others found no significant differences in myocardial mass between wild-type and myostatin-disrupted mice [16, 21, 22]. One study reported signs of dilated cardiomyopathy at rest, including lower strain measurements in myostatin-null mice compared with wild-type mice [18]. Interestingly, however, adrenergic stimulation with isoproterenol revealed enhanced responsiveness in aged myostatin-null mice [18], a sign of increased maximal cardiac functional reserve. Still others have found the myocardial function to be normal [19, 20]. The reasons for these differences in the results from different laboratories are not entirely clear, but differences in mouse strains, experimental models, and measurement techniques could contribute to heterogeneity of results.

Accordingly, we determined the effects of an ActRIIB Fc fusion protein (ActRIIB.Fc)-mediated inhibition of myostatin and other TGF-β/activin family members on myocardial mass and cardiac function using a primate model of acquired immunodeficiency syndrome. The primary aim of this project was to test the hypothesis that administration of ActRIIB.Fc ligand trap would reverse the weight loss and muscle wasting that occurs with the development of acquired immunodeficiency syndrome in SIV-infected juvenile rhesus macaques. Juvenile macaques experience a failure to thrive when inoculated with SIV similar to that observed in HIV-infected children [23], and the SIV model closely parallels the human disease [24, 25]. The results of the efficacy analyses demonstrating the reversal of SIV-associated loss of body weight and muscle mass by ActRIIB.Fc administration have been published [11], as have its effects in bone mineral content and density [26]. Here we describe the results of the prespecified secondary analyses of the cardiac safety data, assessed using two-dimensional echocardiography.

1. Methods

The detailed study protocol has been published [11]. The study protocol was approved by Harvard Medical School's Standing Committee on Animals. The animals were pair-housed in a centralized Animal Biological Safety Level 2 facility at the New England Primate Research Center and were maintained in accordance with the Guide for the Care and Use of Laboratory Animals (Institute for Laboratory Animal Research, 2011). The macaques were fed a certified commercial primate diet (8714; Teklad, Harlan Laboratories, South Easton, MA) and provided fresh water *ad libitum*.

A. Animals

Fourteen male juvenile (2.5 to 3 years) rhesus macaques (*Macaca mulatta*) were studied. Animals were allocated randomly balancing the groups for age and major histocompatibility complex status. The macaques were intravenously inoculated with SIVmac239 (50 ng of p27 viral-antigen equivalent); the day of inoculation was considered day 1. Seven macaques were assigned to receive either ActRIIB.Fc (10 mg/kg/wk), an experimental grade ligand trap

kindly provided by Dr. Carl Morris (Pfizer, Inc., Cambridge, MA), or a saline placebo by intramuscular injection weekly for 12 weeks starting 4 weeks after SIV inoculation.

B. Echocardiography

Two-dimensional and spectral Doppler echocardiography was performed at baseline (week 4) and after 12 weeks of intervention (16 weeks postinoculation). Animals were sedated with Telazol 5 mg/kg intramuscularly before echocardiography. M-mode, two-dimensional echocardiograms were performed by a veterinary cardiologist (Nancy Morris, DVM), who was blind to treatment allocation of animals. Each animal underwent a comprehensive transthoracic scanning with two-dimensional, M-mode, and pulsed-wave Doppler echocardiography using an ultrasound system (General Electric Vivid P, GE Medical Systems Ultrasound and Primary Care Diagnostics, LLC, Wauwatosa, WI). Digital echocardiographic images were captured and stored for later analysis; both still images and digital loops containing three cardiac cycles were saved. The best images captured on each animal were used to perform replicate measurements of each parameter, using leading edge measurement technique to obtain an average value. End-systolic and end-diastolic left ventricular (LV) dimensions and interventricular septum thickness and LV posterior wall thickness in systole and diastole were measured using M-mode tracing from the right parasternal short-axis views. Heart rates were recorded on each monkey. Fractional shortening (FS), ejection fraction (EF), cardiac output, cardiac index, end-diastolic volume, end-systolic volume, and stroke volume were calculated from LV diastolic and systolic measurements, using Teichholz methodology, in accordance with echocardiography guidelines published by the American Society of Echocardiography guidelines [27]. Left atrial maximal dimension and aortic root diameter were measured by M-mode echocardiography from the parasternal long-axis view. Color flow Doppler was used to interrogate pulmonary, aortic, mitral, and tricuspid valves to screen for leaks in valves. Pulsed-wave Doppler was used to determine peak aortic and pulmonary flow velocities. The left parasternal images were used to measure peak mitral E and A inflow velocities.

C. Western Blot Analyses

LV samples were obtained from midventricular short axis of the hearts during euthanasia and frozen at −80°C until analyzed. Pulverized LV muscle was homogenized in 1× cell lysis buffer (#9803; Cell Signaling Technology, Beverly, MA) supplemented with 0.1% SDS and 1 mM phenylmethane sulfonyl fluoride. Primary antibodies for calsequestrin (RRID: AB_2071448) [28] and β-actin (RRID: AB_2714189) [29] were obtained from Santa Cruz Biotechnology, Santa Cruz, CA. Antibodies for phospholamban (RRID: AB_10949105) [30], phosphorylated phospholamban (Ser16/Th17; RRID: AB_10949102) [31], sarcoplasmic calcium ATPase (SERCA)-1 (RRID: AB_2728695) [32], SERCA2a (RRID: AB_10827913) [33], protein kinase A-catalytic α subunit (RRID: AB_10706172) [34], and phospho-protein kinase A-catalytic α (PKA-Cα) (RRID: AB_10707163) [35] were obtained from Cell Signaling Technology. Proteins were separated by SDS-PAGE, transferred to a polyvinylidene difluoride membrane, blocked in 5% milk, and incubated with the first antibody overnight at 4°C with gentle shaking using a 1:1000 dilution ratio. The membrane was washed and incubated in second antibody at room temperature for 1 hour at a 1:4000 dilution ratio. Proteins were detected by exposure to X-ray film after incubation with LumiGLO (#7003; Cell Signaling Technology) and quantified by densitometry using National Institutes of Health ImageJ software.

D. RT-qPCR

Pulverized LV muscle was homogenized in Trizol (#15596018; Invitrogen, Carlsbad, CA) and RNA was extracted using the RNeasy plus mini kit (#74134; Qiagen, Valencia, CA). Residual genomic DNA was removed using the vendor-provided genomic DNA eliminator columns. Single-strand cDNA was synthesized using ProtoScript First Strand cDNA Synthesis Kit (#E6300S; New England Biolabs, Ipswich, MA) following the manufacturer's instruction.

SYBR-based quantitative PCR was performed using a 7500 Sequence Detection System (Thermo Fisher Scientific, Waltham, MA). The primer sequences are listed in Supplemental Table 1.

E. Histopathology

For the histopathological evaluation of the left ventricle for myocardial fibrosis, the tissue was removed immediately after euthanasia and midventricular short-axis heart section fixed in 4.0% paraformaldehyde neutral buffer solution. Tissues were dehydrated, embedded in paraffin, sectioned at a 2-μm thickness, and stained using Masson's trichrome. The relative extent of cardiac fibrosis within each sample was evaluated by an experienced pathologist using a light microscope and scored as 0, 1, or 2 for no, medium, or high myocardial fibrosis, respectively. Digital evaluation of fibrosis was also performed. Three randomly selected fields were analyzed digitally for each sample. The trichrome-stained sections were scanned in an inverted microscope (Eclipse TE2000, Nikon Instruments Inc., Melville, NY) equipped with a SPOT 7.4 Slider RTKE camera (Diagnostic Instruments Inc., Sterling Heights, MI). Images at ×20 magnification were used for digital quantification analysis. Percent fibrosis was determined using the batch mode of the ImageJ software macro [36].

F. Statistical Analyses

Baseline characteristics of animals at week 4 are expressed as mean and SDs. Analysis of covariance with an intervention factor (ActRIIB.Fc or saline), adjusted to baseline value, was performed to assess the effect of intervention at week 16. Echocardiographic measures of myocardial mass and function were calculated as the change from baseline. Sensitivity analyses excluding two animals with early onset of puberty were conducted to investigate robustness of our findings. Unpaired *t* test was used for comparison between expression levels of myocardial mRNA and proteins between treatment arms. All data in graphs are presented as mean ± SEM. Statistical analyses were performed using Prism (version 4.0c; GraphPad Software Incorporated, La Jolla, CA) and SAS software (version 9.3; SAS Institute, Cary, NC).

2. Results

A. Baseline Characteristics and Overall Health

As reported previously, one animal demonstrating rapid progression to simian AIDS in the active intervention arm was euthanized at 14 weeks after SIV inoculation and excluded from analysis [11]. This event was consistent with the expected 5% incidence of rapid progression following inoculation with SIVmac239 [37]. No other animals showed any signs of clinical illness. The analytical sample for the echocardiographic safety analysis included all 13 animals, which had baseline and week 16 echocardiography. As reported previously, two animals (one in each intervention group) developed unusually high serum testosterone levels that were higher than those in the other animals [26], suggestive of earlier than expected onset of puberty. We performed additional sensitivity analyses after excluding these two animals with early onset of puberty, and the results were similar (Supplemental Table 2).

Because of the differences in age and baseline body weight in both groups, there was some variation in baseline measures of cardiac dimensions and function in both groups (Table 1). The plasma SIV copy numbers, $CD4^+$ and $CD8^+$ T lymphocyte counts, body weight, and body composition were similar between the two groups, as was reported previously [11].

B. Effects on Myocardial Mass and Chamber Size

Mean ± SEM cardiac weight at necropsy was slightly higher in ActRIIB.Fc-treated animals (22.5 ± 2.2 g in ActRIIB *vs.* 18.9 ± 2.6 g in the placebo group), but the difference was not

Table 1. Baseline Characteristics of the Animals

	ActRIIB.Fc (n = 6)	Control (n = 7)
Somatometrics		
Body weight, kg	4.2 ± 0.4	3.9 ± 0.7
Body surface area, cm^2	2516 ± 156	2376 ± 219
Cardiac dimensions		
LV internal diameter at diastole, cm	1.80 ± 0.12	1.71 ± 0.18
LV internal diameter at systole, cm	1.10 ± 0.16	1.04 ± 0.15
Interventricular septum thickness at diastole, cm	0.42 ± 0.03	0.41 ± 0.03
Interventricular septum thickness at systole, cm	0.67 ± 0.12	0.65 ± 0.09
LV posterior wall thickness at diastole, cm	0.41 ± 0.04	0.40 ± 0.04
LV posterior wall thickness at systole, cm	0.63 ± 0.09	0.65 ± 0.02
Left atrium diameter, cm	1.10 ± 0.13	1.10 ± 0.13
Aortic root diameter, cm	0.96 ± 0.04	0.93 ± 0.08
Left atrium:aorta ratio	1.16 ± 0.15	1.19 ± 0.12
Cardiac function		
Heart rate, beats/min	140 ± 15	147 ± 21
End-diastolic volume, mL	9.8 ± 1.7	8.6 ± 2.2
End-diastolic volume index, mL/m^2	0.0039 ± 0.0007	0.0036 ± 0.0007
Stroke volume, mL	7.0 ± 1.3	6.2 ± 1.6
End-systolic volume, mL	2.8 ± 1.2	2.4 ± 0.9
End-systolic volume index, mL/m^2	0.0011 ± 0.0005	0.0010 ± 0.0004
Fractional shortening, %	38.6 ± 6.7	38.9 ± 4.8
Ejection fraction, %	71.6 ± 8.2	72.5 ± 6.0
Cardiac output, mL/min	961 ± 105	899 ± 187
Cardiac index, $mL/min/m^2$	0.384 ± 0.046	0.378 ± 0.069

Data are displayed as mean ± SD of characteristics at week 4 (before treatment initiation), except for plasma SIV copy number, which represents quantification at week 2. The baseline data on body weight and body surface area have been reported previously [25] and are shown here only to provide a perspective of the myocardial dimensions in relation to the animal's body size.
Abbreviations: LV, left ventricular; SIV, simian immunodeficiency virus.

statistically significant ($P = 0.199$). Additionally, the ratio of heart weight to total body weight was similar between groups (4.9 ± 0.4% in ActRIIB.Fc group *vs.* 4.8 ± 0.2% in placebo group; $P = 0.832$), suggesting that the slightly increased myocardial mass was proportional to the ActRIIB.Fc-induced increase in body weight. Compared with the placebo injection, the administration of ActRIIB.Fc was associated with a significantly greater increase in the interventricular septal thickness during diastole ($P = 0.010$; Table 2) and systole ($P = 0.036$) (Fig. 1). Similarly, the LV posterior wall thickness increased more in the ActRIIB.Fc-treated macaques than in vehicle-treated animals both during diastole ($P = 0.002$) and systole ($P = 0.044$; Fig. 1). However, the changes in the LV internal diameter did not differ significantly between the two intervention groups either during diastole ($P = 0.555$) or during systole ($P = 0.290$; Fig. 1). The two intervention groups also did not differ significantly in the changes from baseline in left atrial and aortic root dimensions.

C. Effects on Measures of Myocardial Contractile Function

There was a greater increase in heart rate in ActRIIB.Fc-treated animals compared with the placebo-treated animals ($P = 0.015$). The change in cardiac output from baseline was numerically greater in animals treated with ActRIIB.Fc, but between-group differences were not statistically significant ($P = 0.125$; Fig. 2). The changes in cardiac index (cardiac output divided by body surface area) did not differ significantly between the two groups ($P = 0.328$; Fig. 2; Table 2), suggesting that the changes in cardiac output were proportional to the change in body size in the two groups. The EF changed minimally from baseline, and the changes did not differ significantly between groups ($P = 0.153$). Similarly, the two groups did not differ in either the change in stroke volume ($P = 0.770$) or in FS (Fig. 2). The changes in end-diastolic

Table 2. Change From Baseline in Measures of Cardiac Dimensions and Cardiac Function by Treatment Arm

	ActRIIB.Fc	Control	Difference	*P* Value
Somatometrics				
Body weight, kg	0.526 ± 0.112	0.049 ± 0.104	0.477 ± 0.156	0.012
Body surface area, cm^2	186.2 ± 46.8	52.1 ± 43.1	134.1 ± 65.9	0.069
Cardiac dimensions				
LV internal diameter at diastole, cm	0.013 ± 0.053	0.058 ± 0.049	−0.045 ± 0.073	0.555
LV Internal diameter at systole, cm	−0.105 ± 0.044	−0.037 ± 0.041	−0.068 ± 0.061	0.290
Interventricular septum thickness at diastole, cm	0.113 ± 0.024	0.008 ± 0.023	0.105 ± 0.033	0.010
Interventricular septum thickness at systole, cm	0.105 ± 0.037	−0.020 ± 0.034	0.124 ± 0.051	0.036
LV posterior wall at diastole, cm	0.109 ± 0.022	−0.013 ± 0.020	0.122 ± 0.030	0.002
LV posterior wall at systole, cm	0.169 ± 0.046	0.022 ± 0.043	0.146 ± 0.063	0.044
Left atrium diameter, cm	0.173 ± 0.058	0.044 ± 0.053	0.129 ± 0.079	0.133
Aortic root diameter, cm	0.032 ± 0.027	0.005 ± 0.025	0.027 ± 0.037	0.489
Left atrium:aorta ratio	0.137 ± 0.058	0.043 ± 0.054	0.094 ± 0.080	0.268
Cardiac function				
Heart rate, beats/min	28.2 ± 8.7	−7.1 ± 8.0	35.3 ± 12.0	0.015
End-diastolic volume, mL	−1.17 ± 1.05	0.97 ± 0.97	−2.14 ± 1.46	0.174
End-diastolic volume index, mL/m^2	−0.0007 ± 0.0004	0.0003 ± 0.0004	−0.001 ± 0.0006	0.078
Stroke volume, mL	1.07 ± 0.67	0.79 ± 0.62	0.28 ± 0.93	0.770
End-systolic volume, mL	−0.689 ± 0.238	−0.148 ± 0.220	−0.542 ± 0.328	0.129
End-systolic volume index, mL/m^2	−0.0003 ± 0.0001	−0.00006 ± 0.00009	−0.0003 ± 0.0001	0.054
Fractional shortening, %	6.54 ± 1.88	4.20 ± 1.74	2.34 ± 2.56	0.381
Ejection fraction, %	7.47 ± 2.36	2.49 ± 2.18	4.98 ± 3.22	0.153
Cardiac output, mL/min	390.7 ± 133.8	82.1 ± 123.6	308.6 ± 184.2	0.125
Cardiac index, $mL/min/m^2$	0.106 ± 0.049	0.037 ± 0.046	0.069 ± 0.067	0.328

Estimated means and 95% CIs by treatment arm and for the difference between groups. Effects expressed as change from baseline and derived from the analysis of covariance model. *P* value for difference between groups in changes from baseline.
Abbreviations: CI, confidence interval; LV, left ventricular.

and end-systolic volumes did not differ between groups ($P = 0.174$ and 0.129 for end-diastolic and end-systolic volumes, respectively) with or without correction for body mass (Table 2).

D. Effects on the Expression Levels of Myocardial Proteins

Because one animal in each group had signs of early-onset puberty, we excluded these animals from the analyses on expression levels of myocardial proteins because higher testosterone levels might potentially independently affect myocardial gene expression. The RT-quantitative PCR analyses of LV myocardial tissue revealed reduced mRNA expression level of IGF-1, an important factor in the maintenance of normal cardiac structure and function, in animals treated with ActRIIB.Fc relative to controls. This could be a result of compensatory repression caused by the increase in myocardial mass in the ActRIIB.Fc-treated group. However, the mRNA expression levels of myostatin, its downstream target PAI-1, and inflammation markers IL-6 and TNF-α did not differ between the two groups. The expression of NADH-coenzyme Q reductase, a key protein in the complex I of the mitochondrial electron transport chain, also did not differ between the two groups (Fig. 3).

Sarcoplasmic calcium ATPase in fast-twitching (SERCA1) and slow twitching (SERCA2) cardiac myofibers play an important role in the regulation of contractile function in healthy and diseased heart. Aging-related decline in SERCA2 has been linked to myocardial dysfunction [38, 39]. However, aberrant increase in SERCA1/2 and consequent deregulation of calcium intake are also known to be linked to cardiac hypertrophy [40, 41]. Western analysis of LV myocardial tissue revealed a modestly higher protein levels of

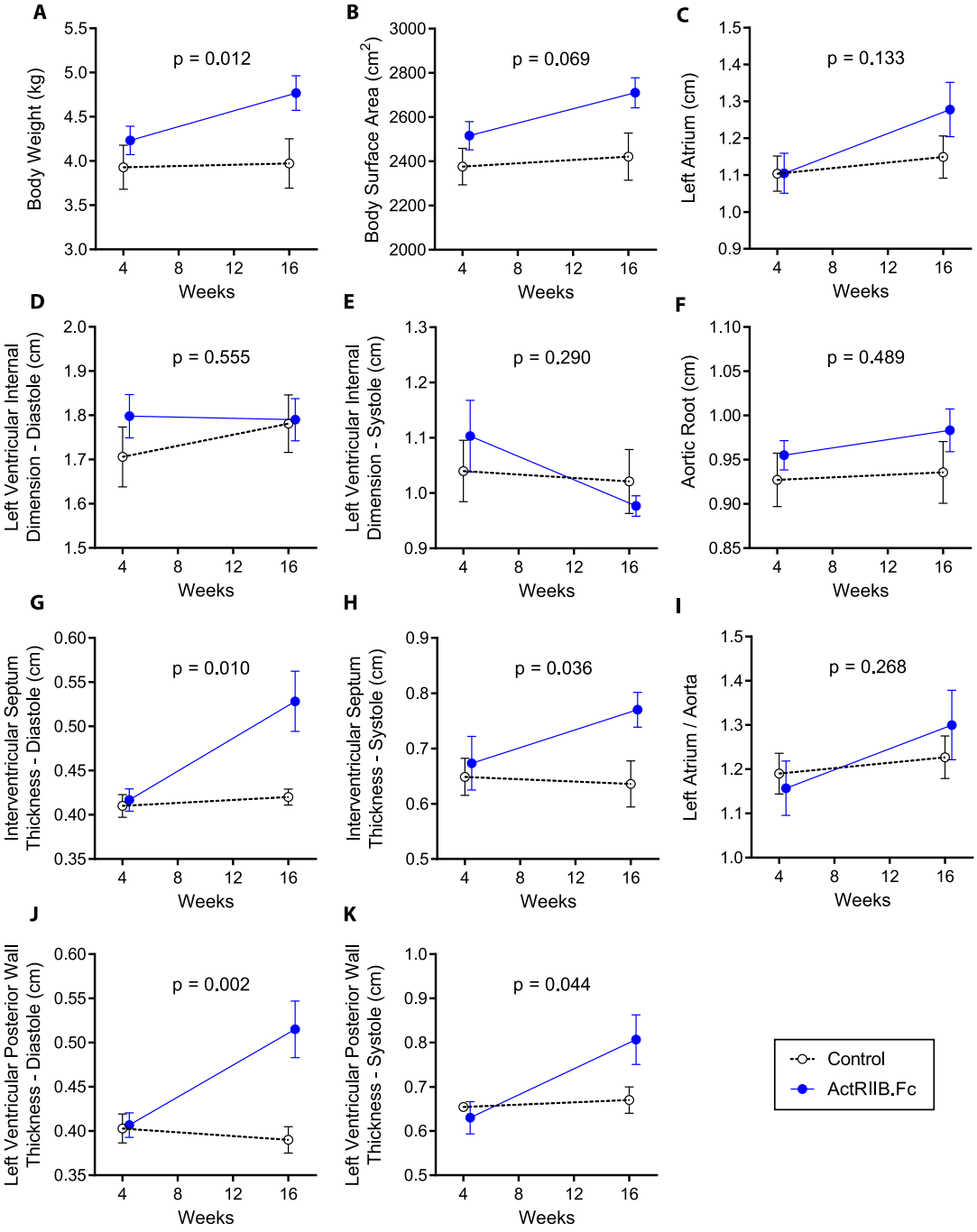

Figure 1. Changes in (A) body weight, (B) body surface area, (C) left atrium, (D) LV internal dimension at diastole, (E) LV internal dimension at systole, (F) aorta, (G) interventricular septum thickness at diastole, (H) interventricular septum thickness at systole, (I) left atrium:aorta ratio, (J) LV posterior wall thickness at diastole, and (K) LV posterior wall thickness at systole in both groups during the study. Data presented are means; error bars are SEM. The weeks represent time after SIV inoculation. Week 4 data represent the baseline data collected 4 weeks after SIV inoculation but immediately before starting the study interventions (ActRIIB.Fc or saline injections); week 16 data represent data collected after 12 weeks of intervention. LV, left ventricular; SIV, simian immunodeficiency virus.

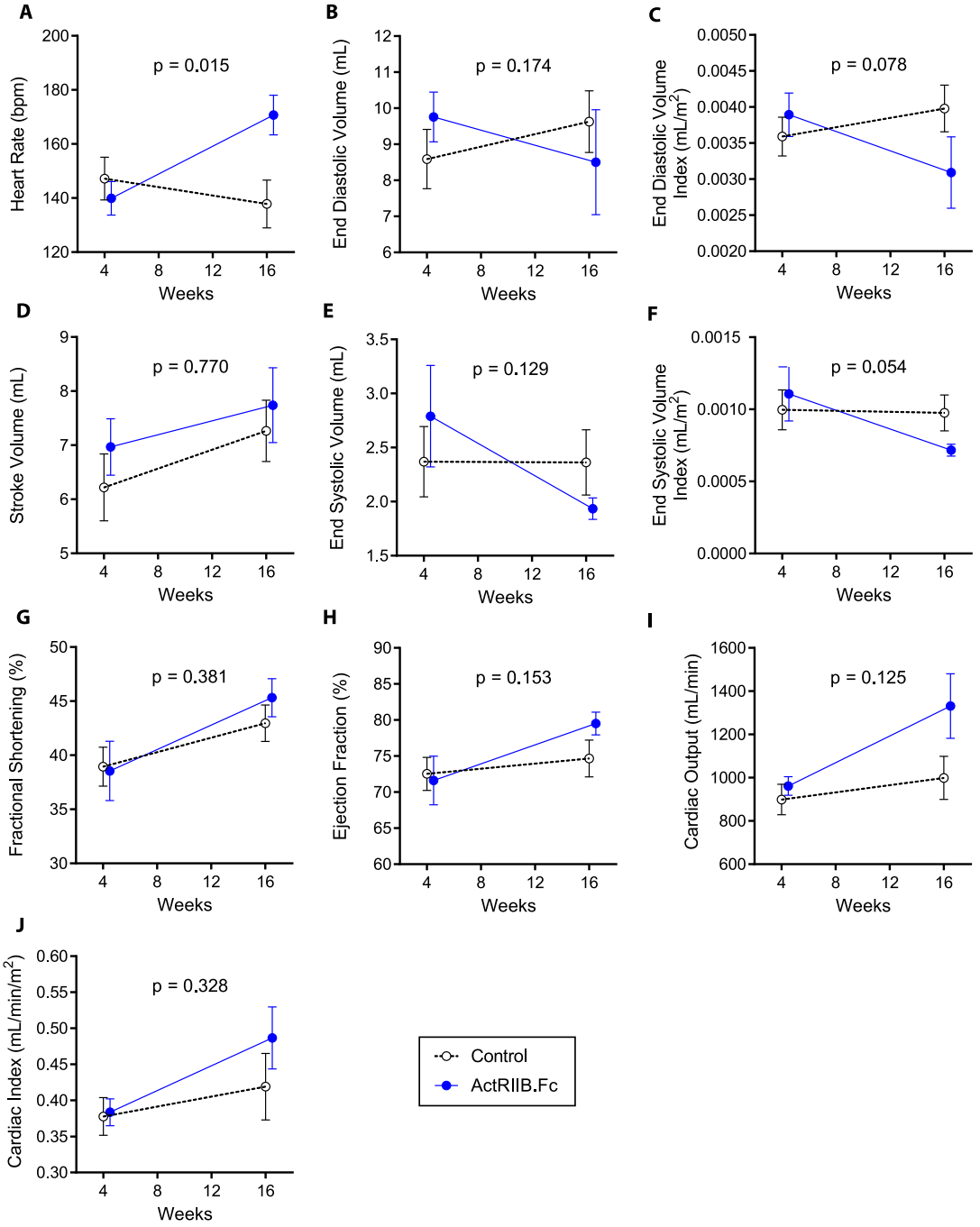

Figure 2. Changes in (A) heart rate, (B) end-diastolic volume, (C) end-diastolic volume index, (D) stroke volume, (E) end-systolic volume, (F) end-systolic volume index, (G) fractional shortening, (H) ejection fraction, (I) cardiac output, and (J) cardiac index in both groups along the study. Data presented are means; error bars are SEM. The weeks represent time after SIV inoculation. Week 4 data represent the baseline data collected 4 weeks after SIV inoculation but immediately before starting the study interventions (ActRIIB.Fc or saline injections).

SERCA1 and SERCA2 in ActRIIB.Fc-treated macaques than in vehicle-treated macaques (Fig. 4), in agreement with prior findings in myostatin-null mice [17, 42]. Phospholamban (PhLB) is a sarcoplasmic reticulum membrane protein that regulates calcium uptake through inhibition of SERCA activity [43–45]. PhLB is negatively regulated by its

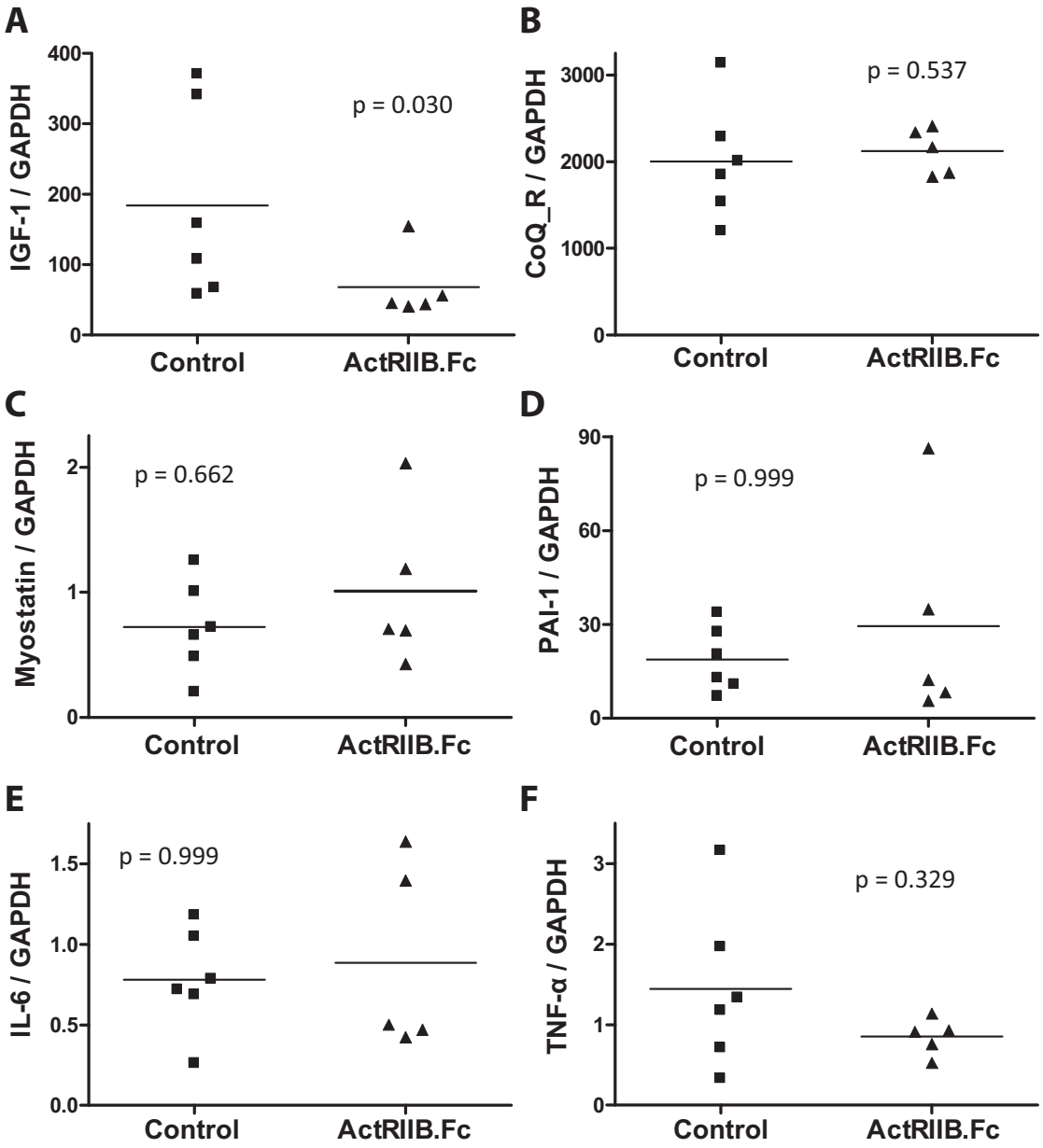

Figure 3. Effects of ActRIIB.Fc or placebo on myocardial expression of (A) IGF-1, (B) NADH-coenzyme Q reductase, (C) myostatin, (D) PAI-1, (E) IL-6, and (F) TNF-α in SIV-infected juvenile male rhesus macaques (n = 5 for ActRIIB.Fc; n = 6 for control). CoQ_R, NADH-coenzyme Q reductase; GAPDH, glyceraldehyde 3-phosphate dehydrogenase.

phosphorylation (Ser16/Th17) mediated by PKA [45, 46]. As shown in Fig. 4, ActRIIB.Fc treatment was associated with an increase in PhLB expression and a decrease in phos-PhLB, which resulted in an even greater decrease in the PhosPhLB:PhLB ratio, suggesting the suppression of SERCA activity. The expression of PKA and phospho-PKA, the upstream kinase that phosphorylates PhLB, did not differ between the placebo and ActRIIB.Fc-treated groups [47].

In addition to the altered expression of PhLB and SERCA1/2, the ActRIIB.Fc-treated group also exhibited a modestly increased expression of calsequestrin, a calcium-binding protein that holds calcium in the cisterna of the sarcoplasmic reticulum. This observation is consistent with similar prior observation in mice [17, 42].

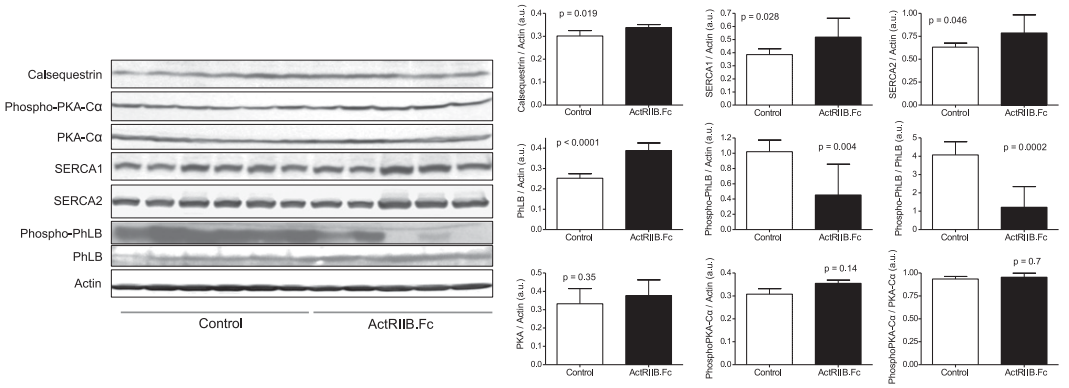

Figure 4. Effects of ActRIIB.Fc or placebo on myocardial protein content of calcium-handling proteins evaluated by western blot. Bars represent means; error bars are SEM of averaged duplicate measurements for each animal (n = 5 for ActRIIB.Fc; n = 6 for control). a.u. = arbitrary units; PhLB, phospholamban; PKA, protein kinase A; SERCA1, sarcoplasmic calcium ATPase in fast-twitching cardiac myofiber; SERCA2, sarcoplasmic calcium ATPase in slow-twitching cardiac myofiber.

E. Effects on Myocardial Fibrosis

Increased cardiomyocyte myostatin expression has been reported to induce myocardial fibrosis [48], and inhibition of the myostatin pathway has been proposed as a potential therapeutic approach for fibrotic cardiomyopathies [49]. Because both SIV and HIV infections have been associated with myocardial fibrosis [50–52], and myostatin expression is increased in HIV [53], we evaluated the effects of ActRIIB.Fc on myocardial fibrosis compared with placebo. Tissue fibrosis was assessed using Masson's trichrome staining. The results were analyzed by visual scoring and by digital quantification. As shown in Fig. 5, there was

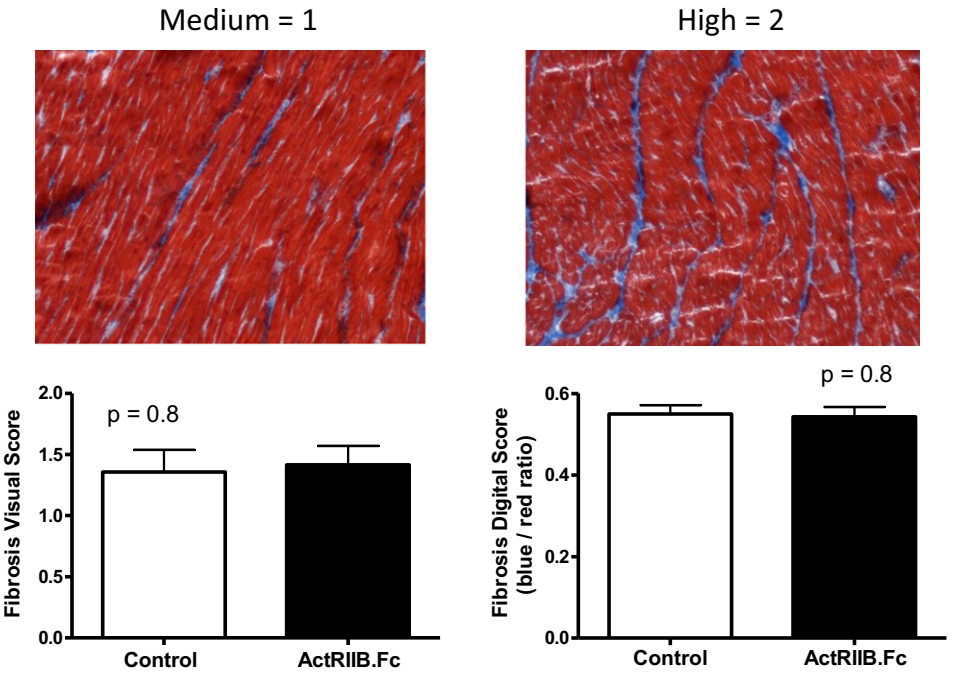

Figure 5. (Top) Examples of medium (left) and high (right) degree of myocardial fibrosis by visual scoring. (Bottom) Means and error bars are SEM for the scores in myocardial fibrosis by visual score (left) and digital score (right).

considerable variation in the level of fibrosis in both groups, with no significant difference in the mean fibrosis score between the two groups, visually or by digital quantification ($P = 0.8$).

3. Discussion

We show here that weekly administration of ActRIIB.Fc for 12 weeks to juvenile SIV-infected rhesus macaques was associated with an increase in some measures of myocardial mass but did not adversely affect overall cardiac function. Additionally, there was no substantial between-group difference in LV myocardial fibrosis or in myocardial expression of inflammatory cytokines IL-6 and TNF-α. However, complex changes were observed in the expression of several important proteins involved in calcium transfer and storage, similar to those reported earlier in the cardiac tissue of myostatin-null mice [42]. These data, together with the previous reports of the effects on the skeletal muscle and bone of SIV-infected macaques [11, 26], suggest that ActRIIB.Fc might be a viable therapeutic option for the treatment of muscle-wasting conditions. Although these findings are reassuring, intervention studies of longer duration are needed to establish the long-term cardiac safety of this class of drugs.

The increased thickness of intraventricular septum and LV posterior wall in ActRIIB.Fc-treated animals compared with control group suggests mild LV hypertrophy, similar to some reports in myostatin-null mice [17–19]. The proportion of myocardial mass to total body weight was similar between the placebo and the treated groups, suggesting that the numerically higher myocardial mass in ActRIIB.Fc-treated animals could be an adaptation to the increased whole-body muscle mass and body weight. However, the changes in LV internal dimensions, stroke volume, EF, and FS were similar between groups, suggesting preserved cardiac function in juvenile macaques treated with ActRIIB.Fc. Similar cardiac remodeling with eccentric hypertrophy is observed in some athletes, particularly in runners, who typically develop thicker LV myocardium without changes in LV chamber volume [54, 55]. This observation differs from the prior observation of an increase in atrial:body weight and ventricle:body weight ratios in transgenic mice expressing a dominant negative myostatin [42, 56]. However, because of the relatively short experimental time frame used in the current study, it remains unknown whether pathological cardiac hypertrophy leading to myocardial dysfunction may develop after prolonged treatment, as found in some studies of myostatin-null mice and the transgenic mice expressing a dominant negative myostatin [18, 56].

Some previous studies in rodents have reported findings suggestive of eccentric hypertrophy with myostatin disruption [17, 18]. Rodgers *et al.* observed that 7-month-old myostatin-null mice had increased LV myocardial mass, as well as increased LV internal volume at diastole and systole, although stroke volume was similar between the myostatin-null mice and the wild-type mice [17]. Adrenergic stimulation with isoproterenol increased stroke volume in myostatin-null mice, contrasting with the reduction observed in wild-type mice [17], suggesting increased stress-induced relaxation and contractile capacity, a characteristic feature of physiologic myocardial hypertrophy. Similar findings were later reported by Jackson *et al.* in aging (13 months of age) myostatin-null mice [18]. Some other studies in rodents have reported the absence of LV hypertrophy with myostatin disruption [20–22]. Interestingly, baseline chamber dimensions and cardiac function in young (8 to 10 weeks old) myostatin-null mice were similar to wild-type [16], whereas in 27- to 37-month-old myostatin-null mice, LV chamber was smaller and FS was greater than in wild-type mice [20]. Taken together, these findings in mice suggest that myostatin disruption leads to the development of mild LV hypertrophy early in adulthood that diminishes with aging, whereas functional (contractile) reserve progressively increases compared with wild-type animals [18]. The cardiac phenotype observed in juvenile macaques treated with ActRIIB.Fc in the current study is similar to the mild cardiac hypertrophy reported in young adult myostatin-null mice.

The slightly numerically higher cardiac output in the ActRIIB.Fc group was not statistically different from that in the control group, and could be largely explained by the higher heart rate in those animals during the week 16 examination. We do not know if this difference

in heart rate was compensatory to the increased oxygen demand associated with the treatment-induced gain in lean body mass [11] or whether this was an incidental finding. We observed changes in the expression pattern of proteins related to myocardial calcium regulation and contractility that suggest increased myocardial contractile activity; these are in agreement with previous observations in myostatin-null mice [42] and reflect the expected action of ActRIIB.Fc. The increase in myocardial SERCA2 and calsequestrin protein levels, along with decreased abundance of phosphorylated phospholamban, are not dissimilar from the alterations in myocardial SERCA2 function observed with exercise training [57]; reduced SERCA2 expression is associated with impaired cardiac function [58], and cardiac SERCA2 and calsequestrin protein levels decrease with aging [38, 59]. However, the changes in SERCA2 and calsequestrin protein levels and the between-group differences in the expression levels of these proteins were small and could have been a chance finding.

We did not observe significant differences in myocardial fibrosis in macaques treated with ActRIIB.Fc, similar to the observations by Cohn *et al.* in a dystrophin-deficient myostatin-null mouse model [21]. Moreover, the transcript levels of cytokines IL-6 and TNF-α were not significantly different between groups. These cytokines as well as myostatin have been previously implicated in myocardial fibrosis [48, 60, 61].

The current study reports the cardiac effects of ActRIIB.Fc treatment in a nonhuman primate model. The study, however, had some limitations. The sample size was small, which might have resulted in a lack of power do detect small between-group differences. The intervention duration of 12 weeks was relatively short. Additionally, it included male macaques only; the cardiac effects of myostatin signaling disruption in mice has been shown to have substantial sexual dimorphism, particularly on cardiac function [18] and on cardiac expression of some calcium-handling proteins [42]. Nonetheless, the preserved myocardial function and the absence of substantial myocardial fibrosis in ActRIIB.Fc-treated male juvenile macaques in this proof-of-concept study are reassuring and suggest that short-term treatment with ActRIIB.Fc does not impair myocardial function.

In conclusion, weekly intramuscular administration of ActRIIB.Fc at 10 mg/kg for 12 weeks to juvenile SIV-infected rhesus macaques was associated with an increase in some measures of myocardial mass, but did not adversely affect overall myocardial function, suggesting mild myocardial hypertrophy. Further studies of longer duration in a larger number of animals of both sexes are needed to establish the long-term cardiac safety and efficacy of ActRIIB.Fc for muscle-wasting conditions. We have previously reported that this ActRIIB.Fc ligand trap was efficacious in increasing whole body and regional lean body mass; reversing SIV-associated weight loss and promoting body weight gain; and in preventing SIV-associated bone loss and increasing bone mineral content with treatment effect sizes varying from 1.06 to 2.3 SD units [11, 26]. Thus, this ActRIIB.Fc ligand trap is a dual muscle and bone anabolic agent, which would be useful in the treatment of conditions associated with loss of muscle and bone, such as HIV-associated wasting; muscle and bone loss associated with androgen deprivation therapy of men with prostate cancer; and age-associated loss of muscle and bone mass. In light of the reassuring short-term myocardial safety data reported here, randomized trials of the compound are indicated for conditions in which the dual muscle and bone anabolic properties might be valuable.

Acknowledgments

Financial Support: This work was supported by National Institutes of Health Grant DK078512 and the Boston Claude D. Pepper Older Americans Independence Center Grant P30AG031679 (to S.B.). ActRIIB.Fc was generously provided by Dr. Carl Morris, Pfizer, Inc. Ron Desrosiers kindly supplied SIVmac239. Animal care was provided by veterinarian Lynn Wachtman and the veterinary technicians at the New England Primate Research Center (NEPRC). Simian immunodeficiency viral loads were analyzed by Jeff Lifson and Mike Piatak at the National Cancer Institute AIDS and Cancer Virus Program. Necropsy service was provided by Elizabeth Curran at NEPRC.

Current Affiliation: K.E. O'Connell's current affiliation is Takeda Pharmaceuticals Int. Co., Cambridge, Massachusetts 02139. S. Westmoreland's current affiliation is AbbVie Bioresearch Center, Pharmacology and Experimental Toxicology, Worcester, Massachusetts 01605.

Correspondence: Shalender Bhasin, MD, Research Program in Men's Health: Aging and Metabolism, Boston Claude D. Pepper Older Americans Independence Center, Brigham and Women's Hospital, Harvard Medical School, 221 Longwood Avenue, Boston, Massachusetts 01225. E-mail: sbhasin@bwh.harvard.edu.

Disclosure Summary: S.B. reports receiving research grants from NIDDK, NIA, and NINR Novartis, Alivegen, and Regeneron Pharmaceuticals and consultation fees from Novartis, Sanofi and Regeneron. S.W. is an employee of AbbVie Pharmaceuticals, Inc. K.E.O. is an employee of Takeda Pharmaceuticals, Co. The remaining authors have nothing to disclose.

References and Notes

1. Kambadur R, Sharma M, Smith TP, Bass JJ. Mutations in myostatin (GDF8) in double-muscled Belgian Blue and Piedmontese cattle. *Genome Res*. 1997;**7**(9):910–916.
2. Schuelke M, Wagner KR, Stolz LE, Hübner C, Riebel T, Kömen W, Braun T, Tobin JF, Lee SJ. Myostatin mutation associated with gross muscle hypertrophy in a child. *N Engl J Med*. 2004;**350**(26): 2682–2688.
3. McPherron AC, Lee SJ. Double muscling in cattle due to mutations in the myostatin gene. *Proc Natl Acad Sci USA*. 1997;**94**(23):12457–12461.
4. Benny Klimek ME, Aydogdu T, Link MJ, Pons M, Koniaris LG, Zimmers TA. Acute inhibition of myostatin-family proteins preserves skeletal muscle in mouse models of cancer cachexia. *Biochem Biophys Res Commun*. 2010;**391**(3):1548–1554.
5. Zhou X, Wang JL, Lu J, Song Y, Kwak KS, Jiao Q, Rosenfeld R, Chen Q, Boone T, Simonet WS, Lacey DL, Goldberg AL, Han HQ. Reversal of cancer cachexia and muscle wasting by ActRIIB antagonism leads to prolonged survival. *Cell*. 2010;**142**(4):531–543.
6. Zhang L, Rajan V, Lin E, Hu Z, Han HQ, Zhou X, Song Y, Min H, Wang X, Du J, Mitch WE. Pharmacological inhibition of myostatin suppresses systemic inflammation and muscle atrophy in mice with chronic kidney disease. *FASEB J*. 2011;**25**(5):1653–1663.
7. Padhi D, Higano CS, Shore ND, Sieber P, Rasmussen E, Smith MR. Pharmacological inhibition of myostatin and changes in lean body mass and lower extremity muscle size in patients receiving androgen deprivation therapy for prostate cancer. *J Clin Endocrinol Metab*. 2014;**99**(10):E1967–E1975.
8. Wagner KR, Fleckenstein JL, Amato AA, Barohn RJ, Bushby K, Escolar DM, Flanigan KM, Pestronk A, Tawil R, Wolfe GI, Eagle M, Florence JM, King WM, Pandya S, Straub V, Juneau P, Meyers K, Csimma C, Araujo T, Allen R, Parsons SA, Wozney JM, Lavallie ER, Mendell JR. A phase I/II trial of MYO-029 in adult subjects with muscular dystrophy. *Ann Neurol*. 2008;**63**(5):561–571.
9. Campbell C, McMillan HJ, Mah JK, Tarnopolsky M, Selby K, McClure T, Wilson DM, Sherman ML, Escolar D, Attie KM. Myostatin inhibitor ACE-031 treatment of ambulatory boys with Duchenne muscular dystrophy: results of a randomized, placebo-controlled clinical trial. *Muscle Nerve*. 2017; **55**(4):458–464.
10. Grossmann M. Myostatin inhibition: a new treatment for androgen deprivation-induced sarcopenia? *J Clin Endocrinol Metab*. 2014;**99**(10):3625–3628.
11. O'Connell KE, Guo W, Serra C, Beck M, Wachtman L, Hoggatt A, Xia D, Pearson C, Knight H, O'Connell M, Miller AD, Westmoreland SV, Bhasin S. The effects of an ActRIIb receptor Fc fusion protein ligand trap in juvenile simian immunodeficiency virus-infected rhesus macaques. *FASEB J*. 2015;**29**(4):1165–1175.
12. Sharma M, Kambadur R, Matthews KG, Somers WG, Devlin GP, Conaglen JV, Fowke PJ, Bass JJ. Myostatin, a transforming growth factor-beta superfamily member, is expressed in heart muscle and is upregulated in cardiomyocytes after infarct. *J Cell Physiol*. 1999;**180**(1):1–9.
13. Ishida J, Konishi M, Saitoh M, Anker M, Anker SD, Springer J. Myostatin signaling is up-regulated in female patients with advanced heart failure. *Int J Cardiol*. 2017;**238**:37–42.
14. Shyu KG, Ko WH, Yang WS, Wang BW, Kuan P. Insulin-like growth factor-1 mediates stretch-induced upregulation of myostatin expression in neonatal rat cardiomyocytes. *Cardiovasc Res*. 2005;**68**(3): 405–414.
15. Gaussin V, Depre C. Myostatin, the cardiac chalone of insulin-like growth factor-1. *Cardiovasc Res*. 2005;**68**(3):347–349.

16. Morissette MR, Cook SA, Foo S, McKoy G, Ashida N, Novikov M, Scherrer-Crosbie M, Li L, Matsui T, Brooks G, Rosenzweig A. Myostatin regulates cardiomyocyte growth through modulation of Akt signaling. *Circ Res*. 2006;**99**(1):15–24.
17. Rodgers BD, Interlichia JP, Garikipati DK, Mamidi R, Chandra M, Nelson OL, Murry CE, Santana LF. Myostatin represses physiological hypertrophy of the heart and excitation-contraction coupling. *J Physiol*. 2009;**587**(Pt 20):4873–4886.
18. Jackson MF, Luong D, Vang DD, Garikipati DK, Stanton JB, Nelson OL, Rodgers BD. The aging myostatin null phenotype: reduced adiposity, cardiac hypertrophy, enhanced cardiac stress response, and sexual dimorphism. *J Endocrinol*. 2012;**213**(3):263–275.
19. Artaza JN, Reisz-Porszasz S, Dow JS, Kloner RA, Tsao J, Bhasin S, Gonzalez-Cadavid NF. Alterations in myostatin expression are associated with changes in cardiac left ventricular mass but not ejection fraction in the mouse. *J Endocrinol*. 2007;**194**(1):63–76.
20. Morissette MR, Stricker JC, Rosenberg MA, Buranasombati C, Levitan EB, Mittleman MA, Rosenzweig A. Effects of myostatin deletion in aging mice. *Aging Cell*. 2009;**8**(5):573–583.
21. Cohn RD, Liang HY, Shetty R, Abraham T, Wagner KR. Myostatin does not regulate cardiac hypertrophy or fibrosis. *Neuromuscul Disord*. 2007;**17**(4):290–296.
22. Heineke J, Auger-Messier M, Xu J, Sargent M, York A, Welle S, Molkentin JD. Genetic deletion of myostatin from the heart prevents skeletal muscle atrophy in heart failure. *Circulation*. 2010;**121**(3):419–425.
23. Freeman LM, Mansfield KG, Lackner AA, Naumova EN, Gorbach SL. Survival and failure to thrive in the SIV-infected juvenile rhesus monkey. *J Acquir Immune Defic Syndr*. 1999;**22**(2):119–123.
24. Putkonen P, Kaaya EE, Böttiger D, Li SL, Nilsson C, Biberfeld P, Biberfeld G. Clinical features and predictive markers of disease progression in cynomolgus monkeys experimentally infected with simian immunodeficiency virus. *AIDS*. 1992;**6**(3):257–263.
25. Simon MA, Chalifoux LV, Ringler DJ. Pathologic features of SIV-induced disease and the association of macrophage infection with disease evolution. *AIDS Res Hum Retroviruses*. 1992;**8**(3):327–337.
26. Guo W, Pencina KM, O'Connell K, Montano M, Peng L, Westmoreland S, Glowacki J, Bhasin S. Administration of an activin receptor IIB ligand trap protects male juvenile rhesus macaques from simian immunodeficiency virus-associated bone loss. *Bone*. 2017;**97**:209–215.
27. Nagueh SF, Appleton CP, Gillebert TC, Marino PN, Oh JK, Smiseth OA, Waggoner AD, Flachskampf FA, Pellikka PA, Evangelista A. Recommendations for the evaluation of left ventricular diastolic function by echocardiography. *J Am Soc Echocardiogr*. 2009;**22**(2):107–133.
28. RRID: AB_2071448.
29. RRID: AB_2714189.
30. RRID: AB_10949105.
31. RRID: AB_10949102.
32. RRID: AB_2728695.
33. RRID: AB_10827913.
34. RRID: AB_10706172.
35. RRID: AB_10707163.
36. Hadi AM, Mouchaers KT, Schalij I, Grunberg K, Meijer GA, Vonk-Noordegraaf A, van der Laarse WJ, Beliën JA. Rapid quantification of myocardial fibrosis: a new macro-based automated analysis. *Cell Oncol (Dordr)*. 2011;**34**(4):343–354.
37. Westmoreland SV, Halpern E, Lackner AA. Simian immunodeficiency virus encephalitis in rhesus macaques is associated with rapid disease progression. *J Neurovirol*. 1998;**4**(3):260–268.
38. Cain BS, Meldrum DR, Joo KS, Wang JF, Meng X, Cleveland JC Jr, Banerjee A, Harken AH. Human SERCA2a levels correlate inversely with age in senescent human myocardium. *J Am Coll Cardiol*. 1998;**32**(2):458–467.
39. Schmidt U, del Monte F, Miyamoto MI, Matsui T, Gwathmey JK, Rosenzweig A, Hajjar RJ. Restoration of diastolic function in senescent rat hearts through adenoviral gene transfer of sarcoplasmic reticulum Ca(2+)-ATPase. *Circulation*. 2000;**101**(7):790–796.
40. Kalyanasundaram A, Lacombe VA, Belevych AE, Brunello L, Carnes CA, Janssen PM, Knollmann BC, Periasamy M, Gyørke S. Up-regulation of sarcoplasmic reticulum Ca(2+) uptake leads to cardiac hypertrophy, contractile dysfunction and early mortality in mice deficient in CASQ2. *Cardiovasc Res*. 2013;**98**(2):297–306.
41. O'Donnell JM, Fields A, Xu X, Chowdhury SA, Geenen DL, Bi J. Limited functional and metabolic improvements in hypertrophic and healthy rat heart overexpressing the skeletal muscle isoform of SERCA1 by adenoviral gene transfer in vivo. *Am J Physiol Heart Circ Physiol*. 2008;**295**(6):H2483–H2494.

42. Jackson MF, Li N, Rodgers BD. Myostatin regulates tissue potency and cardiac calcium-handling proteins. *Endocrinology*. 2014;**155**(5):1771–1785.
43. Kaneko M, Yamamoto H, Sakai H, Kamada Y, Tanaka T, Fujiwara S, Yamamoto S, Takahagi H, Igawa H, Kasai S, Noda M, Inui M, Nishimoto T. A pyridone derivative activates SERCA2a by attenuating the inhibitory effect of phospholamban. *Eur J Pharmacol*. 2017;**814**:1–8.
44. Smeazzetto S, Armanious GP, Moncelli MR, Bak JJ, Lemieux MJ, Young HS, Tadini-Buoninsegni F. Conformational memory in the association of the transmembrane protein phospholamban with the sarcoplasmic reticulum calcium pump SERCA. *J Biol Chem*. 2017;**292**(52):21330–21339.
45. Akaike T, Du N, Lu G, Minamisawa S, Wang Y, Ruan H. A sarcoplasmic reticulum localized protein phosphatase regulates phospholamban phosphorylation and promotes ischemia reperfusion injury in the heart. *JACC Basic Transl Sci*. 2017;**2**(2):160–180.
46. Behar J, Ganesan A, Zhang J, Yaniv Y. The autonomic nervous system regulates the heart rate through cAMP-PKA dependent and independent coupled-clock pacemaker cell mechanisms. *Front Physiol*. 2016;**7**:419.
47. Wu X, Xu T, Li D, Zhu S, Chen Q, Hu W, Pan D, Zhu H, Sun H. ERK/PP1a/PLB/SERCA2a and JNK pathways are involved in luteolin-mediated protection of rat hearts and cardiomyocytes following ischemia/reperfusion. *PLoS One*. 2013;**8**(12):e82957.
48. Biesemann N, Mendler L, Kostin S, Wietelmann A, Borchardt T, Braun T. Myostatin induces interstitial fibrosis in the heart via TAK1 and p38. *Cell Tissue Res*. 2015;**361**(3):779–787.
49. Walton KL, Johnson KE, Harrison CA. Targeting TGF-β mediated SMAD signaling for the prevention of fibrosis. *Front Pharmacol*. 2017;**8**:461.
50. Thiara DK, Liu CY, Raman F, Mangat S, Purdy JB, Duarte HA, Schmidt N, Hur J, Sibley CT, Bluemke DA, Hadigan C. Abnormal myocardial function is related to myocardial steatosis and diffuse myocardial fibrosis in HIV-infected adults. *J Infect Dis*. 2015;**212**(10):1544–1551.
51. Walker JA, Sulciner ML, Nowicki KD, Miller AD, Burdo TH, Williams KC. Elevated numbers of CD163+ macrophages in hearts of simian immunodeficiency virus-infected monkeys correlate with cardiac pathology and fibrosis. *AIDS Res Hum Retroviruses*. 2014;**30**(7):685–694.
52. Walker JA, Beck GA, Campbell JH, Miller AD, Burdo TH, Williams KC. Anti-α4 integrin antibody blocks monocyte/macrophage traffic to the heart and decreases cardiac pathology in a SIV infection model of AIDS. *J Am Heart Assoc*. 2015;**4**(7).
53. Gonzalez-Cadavid NF, Taylor WE, Yarasheski K, Sinha-Hikim I, Ma K, Ezzat S, Shen R, Lalani R, Asa S, Mamita M, Nair G, Arver S, Bhasin S. Organization of the human myostatin gene and expression in healthy men and HIV-infected men with muscle wasting. *Proc Natl Acad Sci USA*. 1998;**95**(25):14938–14943.
54. Pluim BM, Zwinderman AH, van der Laarse A, van der Wall EE. The athlete's heart. A meta-analysis of cardiac structure and function. *Circulation*. 2000;**101**(3):336–344.
55. Spirito P, Pelliccia A, Proschan MA, Granata M, Spataro A, Bellone P, Caselli G, Biffi A, Vecchio C, Maron BJ. Morphology of the "athlete's heart" assessed by echocardiography in 947 elite athletes representing 27 sports. *Am J Cardiol*. 1994;**74**(8):802–806.
56. Rosenberg MA, Das S, Pinzon PQ, Knight AC, Sosnovik DE, Ellinor PT, Rosenzweig A. A novel transgenic mouse model of cardiac hypertrophy and atrial fibrillation. *J Atr Fibrillation*. 2012;**2**(9):1–15.
57. Kemi OJ, Ceci M, Condorelli G, Smith GL, Wisloff U. Myocardial sarcoplasmic reticulum Ca2+ ATPase function is increased by aerobic interval training. *Eur J Cardiovasc Prev Rehabil*. 2008;**15**:145–148.
58. Andersson KB, Birkeland JA, Finsen AV, Louch WE, Sjaastad I, Wang Y, Chen J, Molkentin JD, Chien KR, Sejersted OM, Christensen G. Moderate heart dysfunction in mice with inducible cardiomyocyte-specific excision of the Serca2 gene. *J Mol Cell Cardiol*. 2009;**47**(2):180–187.
59. Herraiz-Martínez A, Álvarez-García J, Llach A, Molina CE, Fernandes J, Ferrero-Gregori A, Rodríguez C, Vallmitjana A, Benítez R, Padró JM, Martínez-González J, Cinca J, Hove-Madsen L. Ageing is associated with deterioration of calcium homeostasis in isolated human right atrial myocytes. *Cardiovasc Res*. 2015;**106**(1):76–86.
60. Sakata Y, Chancey AL, Divakaran VG, Sekiguchi K, Sivasubramanian N, Mann DL. Transforming growth factor-beta receptor antagonism attenuates myocardial fibrosis in mice with cardiac-restricted overexpression of tumor necrosis factor. *Basic Res Cardiol*. 2008;**103**(1):60–68.
61. Wang JH, Zhao L, Pan X, Chen NN, Chen J, Gong QL, Su F, Yan J, Zhang Y, Zhang SH. Hypoxia-stimulated cardiac fibroblast production of IL-6 promotes myocardial fibrosis via the TGF-β1 signaling pathway [printed correction appears in *Lab Invest*. 2016;96:1035]. *Lab Invest*. 2016;**96**(8):839–852.